ELSEVIER

Solid State Ionics 143 (2001) 161–171

SOLID STATE IONICS

www.elsevier.com/locate/ssi

Boron-substituted manganese spinel oxide cathode for lithium ion battery

A. Veluchamy [a], H. Ikuta [b], M. Wakihara [b,*]

[a] *Central Electrochemical Research Institute, Karaikudi 630006, India*

[b] *Department of Applied Chemistry, Graduate School of Science and Engineering, Tokyo Institute of Technology, 2-12-1 Ookayama, Meguro-ku, Tokyo 152-8552, Japan*

Received 18 June 2000; received in revised form 2 March 2001; accepted 23 March 2001

Abstract

An attempt has been made to synthesize boron-substituted cubic spinel through solid state (SS) and solution route (SR) techniques. The synthesized spinels have been examined for their physical and electrochemical characteristics through ex situ-X-ray diffractometry (XRD) and SEM, as well as by charge–discharge cycling and diffusion coefficient measurements. X-ray diffraction reveals boron elimination from boron-substituted spinel (SR-B spinel) resulting in phase splitting to lithium borate glass formation and parent cubic spinel when subjected to heating at and above 600°C. Synthesis through SR with precursor material calcined at 500°C only provides high discharge capacity with good cyclability. The measurement of diffusion coefficient of lithium supports that boron got substituted at 16*d* site in $Fd\bar{3}m$ spinel structure. This paper discusses the mechanism underlying the stability of boron-substituted spinel and the suitability of $LiB_{1/9}Mn_{17/9}O_4$ as a promising positive electrode candidate for lithium ion battery.

Keywords: Solution route; Cubic spinel; Tetragonal configuration; Lithium borate glass; Lithium ion battery; Diffusion coefficient

1. Introduction

The demand for portable electronic devices necessitates lithium ion batteries with compatible electrochemical output in addition to cost advantage and environmental acceptability. Despite the mixed phase $LiNi_{1-y}Co_yO_2$ [1,2] standing as a serious competitor in place of $LiCoO_2$ [3,4], much attention has been focused recently on $LiMn_2O_4$ [5–10] spinel, as it is a low cost and less toxic material, except for its drawback due to its capacity fade with cycling. $LiMn_2O_4$ belongs to space group $Fd\bar{3}m$, in which lithium ion occupy tetrahedral 8*a* site and manganese ion occupy octahedral 16*d* site. The capacity fade in $Li_xMn_2O_4$ ($0 < x < 1$) spinel is described as due to the weaker Mn−O bond in octahedron [11]. Recent researches reveal that reinforcement of the spinel structure by substituting a part of Mn^{3+}, with Co, Cr, Ni, Al, Cr–Al or Al–Co, prevents capacity fade and results in higher cyclability [12–15]. It has been reported that $LiM_{1/6}Mn_{11/6}O_4$ (M = Cr, Co and Ni) is the best composition, exhibiting better cyclability among various composition ($LiM_yMn_{2-y}O_4$) investigated [12]. It is also observed that a 10% substitution of other metal in 16*d* site in place of Mn is as effective in producing stability to the structure, and it

* Corresponding author. Tel.: +81-3-5734-2145; fax: +81-3-5734-2146.

E-mail address: mwakihar@o.cc.titech.ac.jp (M. Wakihara).

0167-2738/01/$ - see front matter
PII: S0167-2738(01)00856-6

is found that Co-substituted spinel provides high cyclability due to its minimum volume expansion during the charge–discharge process [12,13].

Despite many transition and non-transition elements having been explored as partial substituents, in place of manganese in the cubic spinel, there is no report as far now on boron-substituted spinel compound with pure phase having energy capacity and cycle life behavior comparable to well known substituted spinels. Here, we have attempted to synthesize this boron-substituted spinel through high temperature solid state (SS) synthesis procedure [12], as well by low temperature solution route (SR) synthesis [16,17].

In this paper, we describe the preparative procedure for the synthesis of polycrystalline boron-substituted manganese spinel with pure phase through solution route method, with the aid of polyvinyl alcohol as the gelling agent. Investigation has been made on its thermal stability, diffusion coefficient, substitution site of boron in the spinel, charge/discharge behavior, cyclability, and its suitability to lithium ion battery. This paper also describes the attempt to prepare boron-substituted spinel by solid state synthesis procedure, the cause for its failure to produce proper substitution in the spinel, and a comparison of the performance with the former.

2. Experimental

2.1. Synthesis procedure

The procedure for the high temperature synthesis of boron-substituted spinels is same as that described for the synthesis [12] of substituted spinel using the stoichiometric quantities of materials such as Li_2CO_3, $MnCO_3$ and B_2O_3 (all 99.9%, Soekawa Chemicals).

The reagents used for the boron-substituted spinel through solution route were polyvinyl alcohol (PVA, $n = 1500$) (Wako), lithium nitrate ($LiNO_3$) and manganese acetate tetrahydrate ($Mn(CH_3COO)_2 \cdot 4H_2O$) (Soekawa Chemicals) and boric acid (H_3BO_3) (Triple Benzene Trade Mark, Japan). For the preparation of boron-substituted spinels with composition $LiB_yMn_{2-y}O_4$ ($y = 1/3$, $1/6$, $1/9$, $1/12$), stoichiometric amounts of $Mn(CH_3COO)_2 \cdot 4H_2O$ and H_3BO_3, weighing 3 g in total, were dissolved in 50 ml of distilled water and added to 200 ml of 0.5% PVA solution, prepared by dissolving 1 g of PVA in 200 ml of distilled water and then heating to 60°C under constant stirring. The mixed solution was then heated to about 70°C to evaporate the water content under constant stirring condition, so as to get a final desired viscous solution. The viscous solution was then transferred into an alumina crucible, heated to 300°C in a furnace for about 3 h. The flabby mass obtained was then ground to produce a precursor power. This precursor powder was then heated to 500°C in an air oven using an alumina boat for about 8 h to get the final product. A portion of a precursor powder of $LiB_{1/6}Mn_{11/6}O_4$ was heated to 600°C to obtain the electrochemical characteristics of higher temperature treated material. Following the same procedure, $LiMn_2O_4$ was prepared by using the same materials, but with lithium acetate, $LiOCOCH_3$, in place of lithium nitrate, $LiNO_3$, in a higher percentage (6 g of PVA in 200 ml distilled water) of PVA solution, and the precursor was heated to 600°C to obtain the final product. The boron-substituted spinel obtained through solid state method and solution route are designated as SS-B spinel and SR-B spinel, respectively, for simplicity. Unless otherwise mentioned, the material described in this paper relates only to boron-substituted spinel prepared through solution route with precursor material treated at 500°C for 8 h.

2.2. Cell construction

The synthesized materials were used for the preparation of composite positive electrode materials. The procedures for the fabrication of lithium rechargeable cells are almost the same as those described previously [11,13]. The composite positive electrode materials were prepared by mixing any one of the synthesized compounds in agate mortar with acetylene black, and polytetrafluoroethylene (PTFE) powder in the weight ratio of 75:20:5, respectively. This mixture was pressed into a film with 100-μm thickness. Films weighing 2–3 mg were cut in the form of small discs (5-mm diameter and 2–3-mg weight) and used as the positive electrode. Positive electrode limiting cells were assembled using a spring-loaded stainless steel arrangement, by placing

positive electrode and lithium foil negative electrode (5-mm diameter) separated by a microporous polyethylene separator. The electrolyte used was 1 M $LiClO_4$ dissolved in ethylene carbonate and diethyl carbonate (EC/DEC = 1:1) procured from Tomiyama Pure Chemical. The charge and discharge cut-off voltages were set at 4.4 and 3.5 V, and cycling was performed galvanostatically at a current density of 0.2 mA cm^{-2}.

Cell construction used for the measurement of diffusion coefficient of lithium was the same procedure as described above for the charge–discharge study.

2.3. Ex situ XRD and SEM analysis

The diffraction data on phase identification and lattice parameter were collected at 40 kV/80 mA and 50 kV/100 mA, respectively, over 2θ range from 5° to 120° by powder X-ray diffractometry (XRD) using CuKα radiation with a graphite monochromator through RINT-2500 V, Rigaku. The surface morphology was obtained through SEM micrographs using JSM-5310 LV, JEOL. The sample for measuring the lattice parameter was prepared by mixing four parts of the sample with one part of silicon, and the lattice parameter was calculated using silicon with a diamond structure as an internal reference.

2.4. Current pulse relaxation technique

The current pulse relaxation technique was employed to obtain the apparent chemical diffusion coefficient [14,15,18] of the synthesized compounds and the open circuit voltages (OCV) of the cells measured with respect to lithium negative electrode. The cells were first galvanostatically charged to drive out 0.5 Li from the positive electrode of the cells at 0.1 mA cm^{-2}, so that the final composition of the positive electrode are $Li_{0.5}B_yMn_{2-y}O_4$ and $Li_{0.5}$-Mn_2O_4 for the SR-B spinel and SS-parent spinel, respectively. Then, the following sequence was repeated: (1) given rest time of 6 h at $x = 0.5$, (2) monitored the steady OCV, (3) applied pulse charge voltage (lithiation) at 0.5 mA cm^{-2} for 10 s, (4) monitored the relaxation potential with $t^{-1/2}$, during this period the voltage rises with time, (5) discharged the cell by intercalating 0.03125 parts of lithium at 0.1 mA cm^{-2}. Through this sequence, we obtained 16 values of tan δ values, which are equal to $\Delta E/\Delta t^{-1/2}$. The chemical diffusion coefficient of lithium ion was calculated from the decay rate of the transient voltage using the following equation,

$$\tilde{D} = \frac{1}{\pi}\left[\frac{V_M(dE/dx)}{nFA}\,\frac{i\tau}{\Delta E/\Delta t^{-1/2}}\right]^2, \qquad (1)$$

where, V_M is the molar volume; dE/dx is the slope of the equilibrium potential–composition curve; F is Faraday's constant; t is the pulse duration and $\Delta E/\Delta t^{-1/2}$ is the slope of the straight line obtained from the plot of the relaxation potential vs. $t^{-1/2}$ after the current pulse is stopped. The quasi open-circuit voltage (OCV) was also obtained for every interval period of rest time. All the cell construction and electrochemical measurements were carried out in an Ar-filled glove box at room temperature.

3. Results and discussion

3.1. XRD and SEM analysis

3.1.1. Solid state prepared SR-B spinel

XRD pattern of the cubic spinel ($LiB_{1/6}$-$Mn_{11/6}O_4$), which was intended to be prepared at 750°C followed by slow cooling [12], and the XRD pattern of the same material quenched after heating at 750°C are shown in Fig. 1, represented by (a) and (b), respectively. The materials so prepared were gray colored and hard abrasive type materials, and differ in physical properties from other substituted spinels, $LiM_yMn_{2-y}O_4$ (M = Co, Ni, and Al) prepared by solid state technique. The XRD pattern (a) corresponds to cubic spinel structure, whereas diagram (b) shows that the cubic structure underwent distortion to tetragonal structure.

From the thermochemical data [19], we understood that one of the substance, B_2O_3, used in this preparation has a low melting point of 580°C. Therefore, it can be expected that melting of B_2O_3 could occur before the spinel formation temperature. At spinel formation temperature, this melted B_2O_3 would possibly react with lithium compound to form lithium borate glass, $LiBO_2$. Therefore, the formed

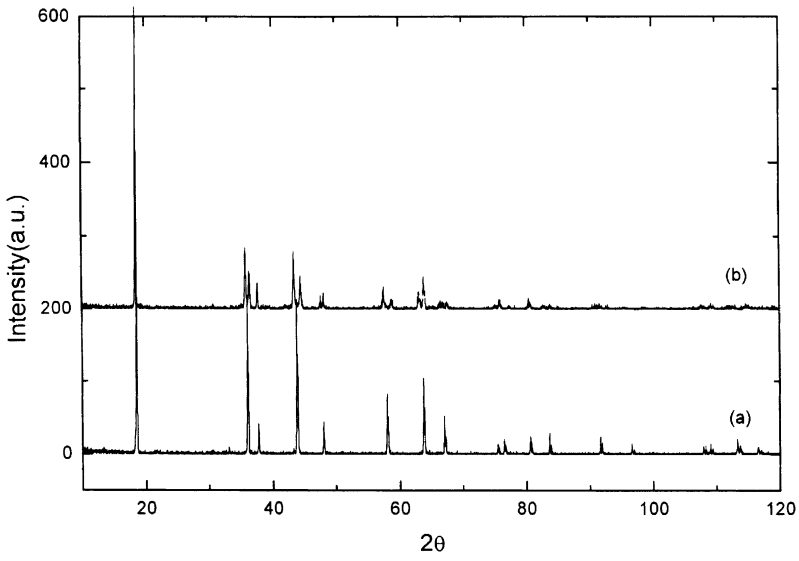

Fig. 1. The XRD pattern of substance obtained after heating the stoichiometric ingredients for the preparation of $LiB_{1/6}Mn_{11/6}O_4$ by solid state reaction at 750°C: (a) on slow cooling; (b) on quenching.

product may, presumably, be a combination of spinel and lithium borate glass ($LiMn_2O_4 + LiBO_2$) [19,20]. Presence of this glass material could provide hardness to the substance, and also create a reducing atmosphere, which may be responsible for the distortion of this compound to tetragonal configuration upon quenching.

3.1.2. Solution route prepared SR-B spinels

XRD patterns of the SR-B spinels (precursor powder heated to 500°C for 8 h) are presented in Fig. 2. These patterns confirm that all the substituted manganese spinels with different levels of boron substitution have cubic spinel phase refined with space group $Fd\bar{3}m$ with no discernable impurities.

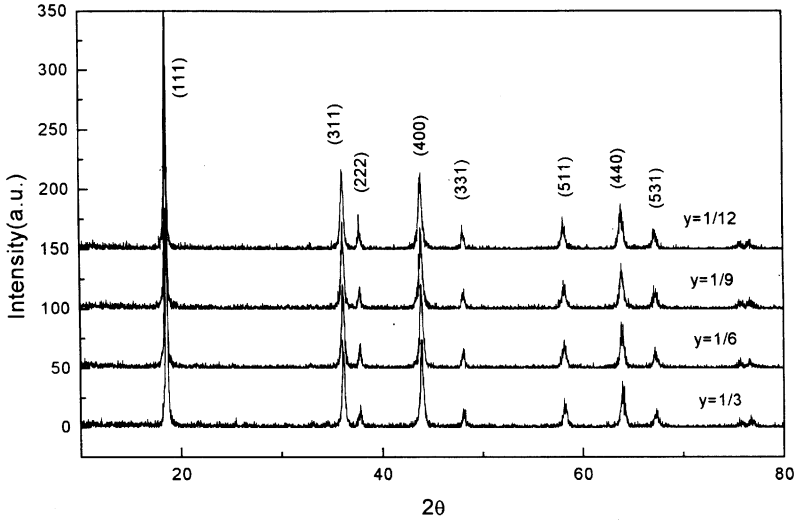

Fig. 2. The XRD patterns of SR-$LiB_yMn_{2-y}O_4$ ($y = 1/3$, $1/6$, $1/9$ and $1/12$).

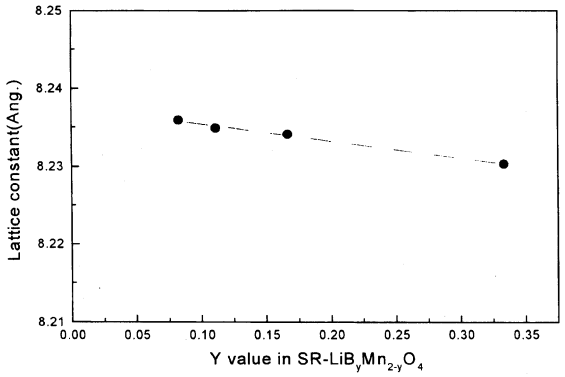

Fig. 3. Dependence of the lattice constant the with y values in SR-$LiB_yMn_{2-y}O_4$ ($y = 1/3$, $1/6$, $1/9$ and $1/12$).

Cubic lattice constant values obtained for SR-B spinels are presented in Fig. 3, where it may be noted that the lattice constants decrease with increase in the substituting level of boron in a linear fashion, showing that the substitution place its role in reducing the cubic spinel size. Let us make an apparent comparison, even though the preparative conditions are different, of the lattice constant of $LiB_{1/6}Mn_{11/6}O_4$ with a few substituted and non-substituted cubic spinels reported [12–15], which will give light on the influence of the boron over the spinel structure. The lattice constant values of Co-, Ni- and Al-substituted spinels, prepared through solid state method at the formation temperature of 750°C are, respectively, 8.215, 8.220 and 8.220 Å, whereas the SR-B spinel (precursor treated at 500°C) has a lattice constant value of 8.234 Å at the same substitution level represented as $LiM_{1/6}Mn_{11/6}O_4$ (M = Co, Ni, Al and B). The cause for smaller lattice constant value of boron-substituted spinel implies that boron, with smaller radius (~ 0.2 Å), could not effectively influence the surrounding oxygen spheres to result in a smaller lattice constant values [21]. This can be better understood when we compare the lattice constant values of $LiB_{1/3}Mn_{5/3}O_4$ and $LiB_{1/12}Mn_{23/12}O_4$, which are 8.230 and 8.236 Å, respectively. The wide substitution results to only a narrow difference in lattice constant value (~ 0.006 Å).

The materials formed for the precursor treated at 500°C were of very fine and high bulk-density nature. The typical SEM photographs shown in Fig. 4 reveal that there is not much difference in particle sizes for different boron substitution levels in the SR-B spinels. This can be correlated with minimum difference in lattice constant values observed among the SR-B spinels. The powders seem to be less crystalline, presumably due to low calcination temperature of the precursor. Again, the photographs show that particle shapes vary widely, showing that the synthesized powders are of polycrystalline nature.

3.1.3. Thermal stability of $LiB_{1/6}Mn_{11/6}O_4$

As most metal oxides of boron are associated with glassy type of materials, and further, the quenched SS-B spinel ($LiB_{1/6}Mn_{11/6}O_4$) after heating to 750°C showed an XRD pattern related to tetragonal structure, we attempted to investigate the stability of SR-B spinel on $LiB_{1/6}Mn_{11/6}O_4$. Several portions of SR-$LiB_{1/6}Mn_{11/6}O_4$ were exposed to different

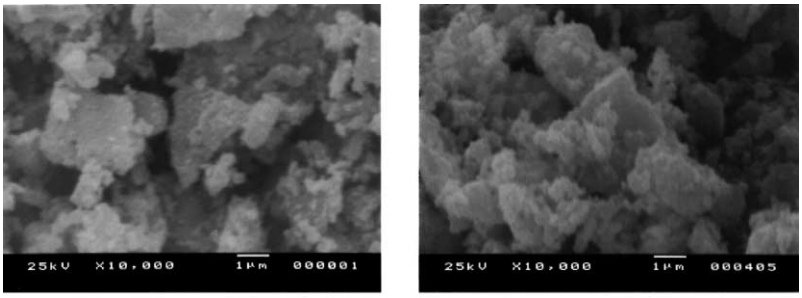

(a) (b)

Fig. 4. SEM photographs for SR-B spinels, precursor treated at 500°C: (a) SR-$LiB_{1/3}Mn_{5/3}O_4$; (b) SR-$LiB_{1/9}M_{17/9}O_4$.

heating temperatures for about 8 h and slow-cooled specifically. The X-ray diffraction patterns obtained were depicted in Fig. 5. For better understanding, the enlarged view of Bragg peaks (311) and (400) are shown in Fig. 6. The figure shows that the Bragg peaks splitting at 600°C are possibly due to the elimination of boron from 16*d* site of the structure, with the simultaneous formation of lithium borate glass and pure spinel. The SR-B spinel prepared at 600°C is hard enough to assume that it consisted of lithium borate glass, and the peak at low 2θ value is related to pure spinel. The original peak corresponding to SR-B spinel almost disappeared, and only a peak related to pure spinel appears at 700°C. At 750°C, two broad peak appears related to distortion of the formed cubic spinel into tetragonal configuration.

Fig. 7 shows variation of lattice constant with exposure temperature. Undoubtedly, the higher lattice constant value reflected in the graph is due to the higher percentage of pure spinel ($LiMn_2O_4$) formed on heating SR-B spinel. The increase in lattice constant also implies decrease in boron content in the spinel. This trend is similar in nature, observed in variation of lattice constant with boron content curve represented in Fig. 3, where at higher value of lattice constant, the boron content is very minimum.

3.2. Electrochemical investigations

3.2.1. Charge / discharge analysis

Charge/discharge studies were performed for all the materials synthesized. For critical analysis, let us consider the typical charge/discharge patterns of the cells represented in Fig. 8. In this figure, the charge/discharge curves for SS-B spinel ($LiB_{1/6}Mn_{11/6}O_4$) prepared at 750°C, SR-B spinel ($LiB_{1/6}Mn_{11/6}O_4$)—precursor calcined at 600°C—and

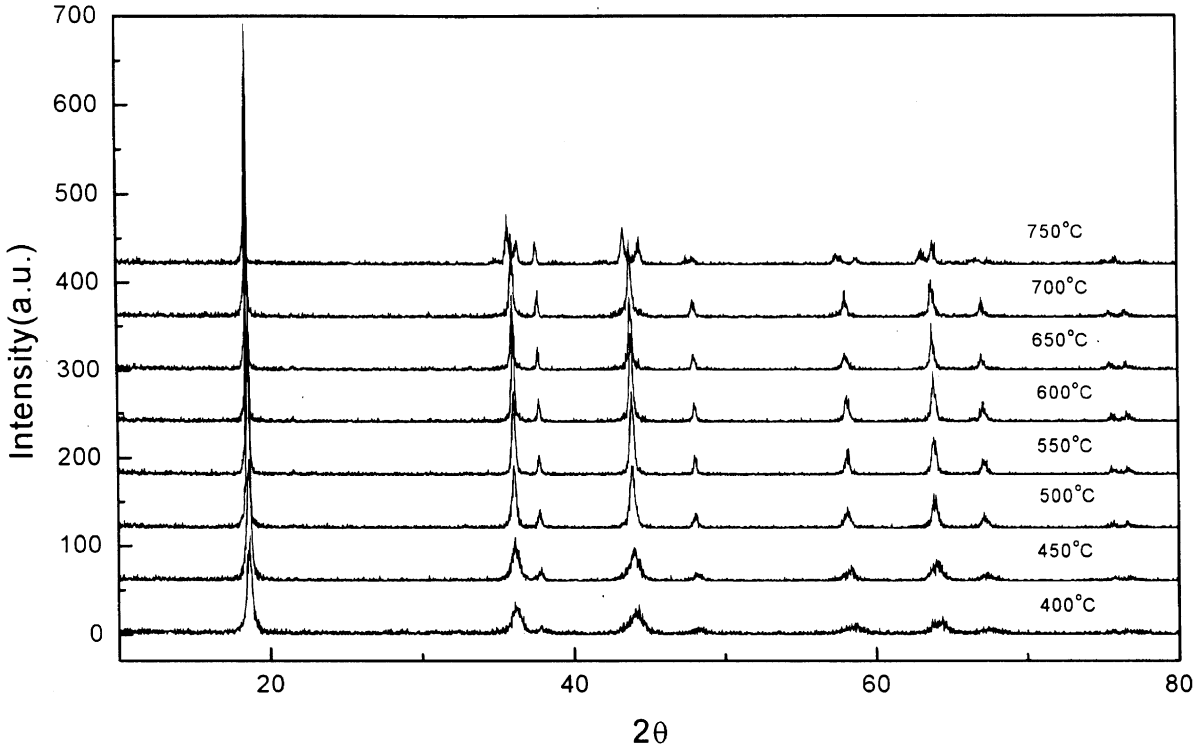

Fig. 5. X-ray patterns of SR-$LiB_{1/6}$ $Mn_{11/6}O_4$ sample exposed to different temperatures.

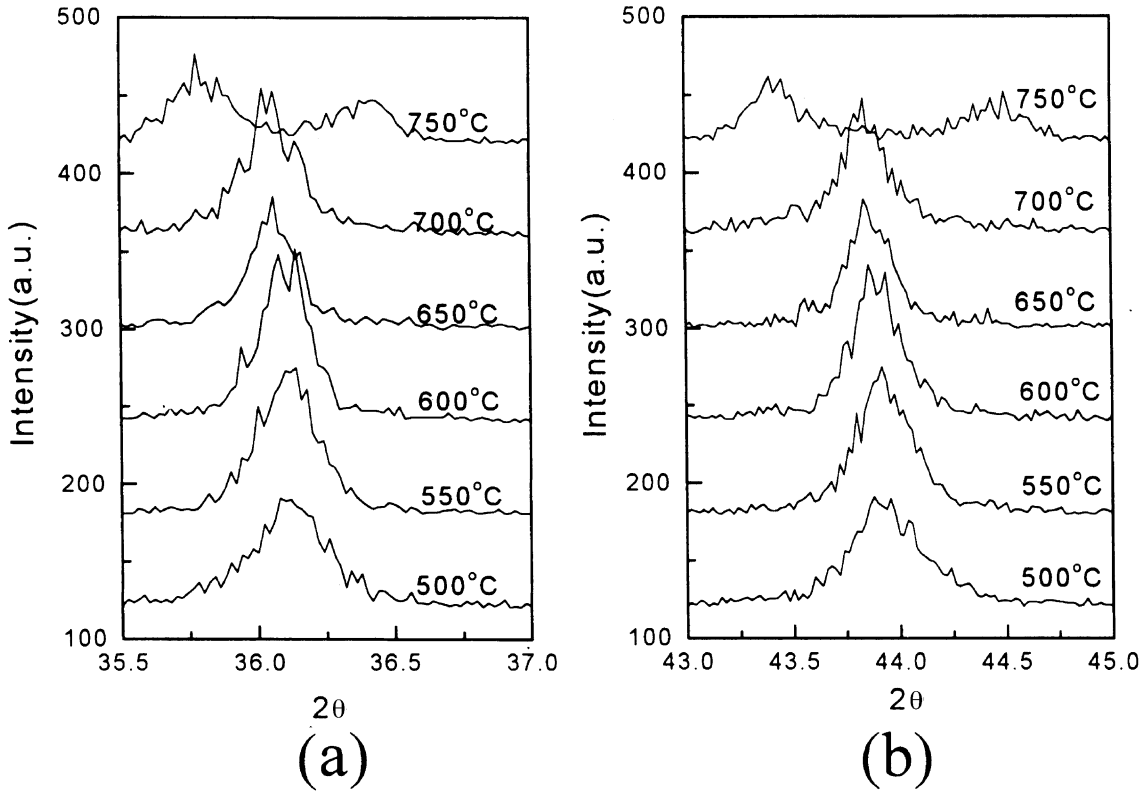

Fig. 6. Shift of Bragg peaks with temperature: (a) (311) plane; (b) (400) plane.

SR-B spinel ($LiB_{1/6}Mn_{11/6}O_4$)—precursor calcined at 500°C—are shown as (a), (b) and (c), respectively.

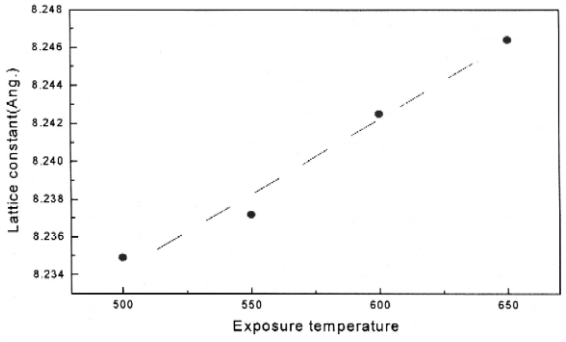

Fig. 7. Dependence of lattice constant with temperature for SR-$LiB_{1/6}Mn_{11/6}O_4$ spinel.

In (a), one may observe that despite a larger charge capacity (120 mA h/g) in the first charging process, it delivers less discharge capacity (<80 mA h/g). This discharge capacity is not even the capacity (100 mA/h) expected corresponding to $Mn^{3+}_{5/6}$ even if one discount the formation of boron-substituted spinel (1/6 portion).

Curves in (b) for SR-$LiB_{1/6}Mn_{11/6}O_4$ spinel (precursor treated at 600°C) show that the pattern is very similar to that of (a). The substance shows an initial of <100 mA h/g and at the 5th cycle the capacity drops to <90 mA h/g.

Curves in (c) for SR-$LiB_{1/6}Mn_{11/6}O_4$ spinel (precursor treated at 500°C) show smooth charge/discharge patterns of spinel. The smooth patterns with maximum initial capacity (>110 mA h/g) with good cycling behavior seems comparable to the best-performing substituted spinel compound $LiCo_{1/6}Mn_{11/6}O_4$ [12,14].

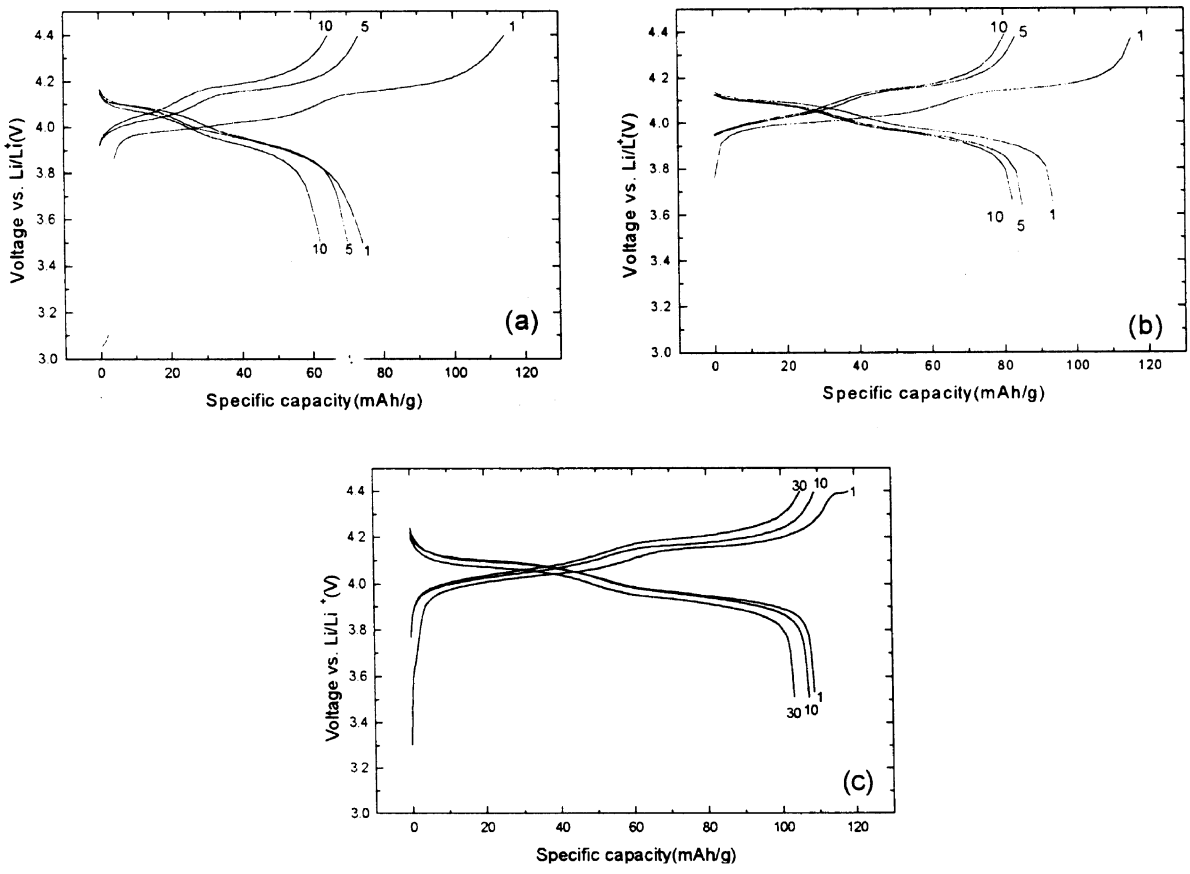

Fig. 8. Charge/discharge curves obtained for cells with (a) substance obtained after heating the stoichiometric ingredients for the preparation of $LiB_{1/6}Mn_{11/6}O_4$ by solid state reaction at 750°C, (b) SR-$LiB_{1/6}Mn_{11/6}O_4$, precursor treated at 600°C, and (c) SR-$LiB_{1/6}Mn_{11/6}O_4$, precursor treated at 500°C.

All these suggest that SR-B spinel, with precursor treated at 500°C, is only suitable for battery application. The high capacity fade that is observed at high temperature prepared samples, as in (a) and (b), may be attributed to the presence of any metastable material present in the sample that transform into stable form on deintercalation.

3.2.2. Cyclability

Fig. 9 compares the accessible capacity of the spinels SR-B $LiB_yMn_{2-y}O_4$ ($y = 1/3$, $1/6$, $1/9$ and $1/12$) and SS-$LiMn_2O_4$ with cycling. The curves show that there is a drop in capacity accessibility with substitution level, for the obvious reason that Mn^{3+} is responsible for capacity realization, which decreases with substitution level. It is evident from the figure that cells with SS-$LiMn_2O_4$, synthesized through solid state reaction, has the highest capacity loss with cycling. To make a clear understanding of the level of capacity fade with cycling for the different substituted spinels, the slope values for all the four substituted spinels were obtained through linear square fit, and are presented in Fig. 10. The figure shows that the loss in capacity is higher for lowest substitution, and is very minimum for the one with higher boron substitution. Of all the SR-B spinel, the one with the composition $LiB_{1/9}Mn_{17/9}O_4$, in addition to sustaining good cycle performance, inherits good capacity value (> 110 mA h/g) comparable with the best-known substituted spinel.

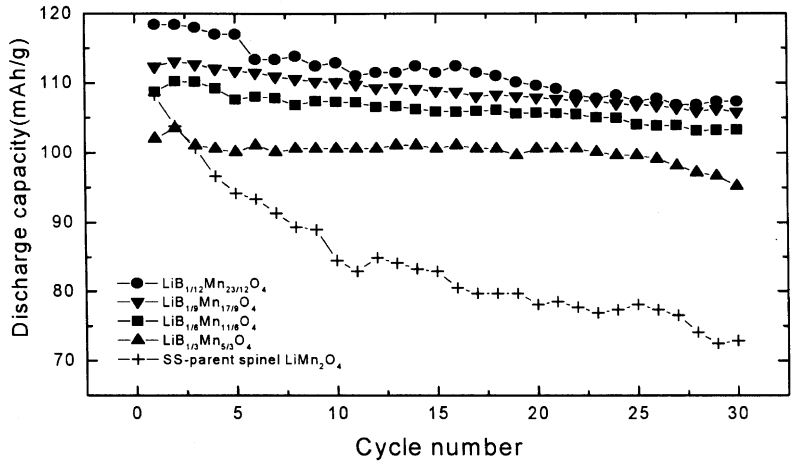

Fig. 9. Variation of capacity with cycle number for the positive electrode materials SR-$LiB_yMn_{2-y}O_4$ ($y = 1/3$, $1/6$, $1/9$ and $1/12$) and SS-$LiMn_2O_4$.

The spectacular cyclability of the substituted spinel may, in general, be explained by the following statements.

(a) The relative stability of parent spinel and boron-substituted spinel could be apparently conceived through the standard Gibbs energy of formation (ΔG_f°) at 298 K of Mn_2O_3 and B_2O_3, which lie at -881 and -1192 kJ mol^{-1}, respectively [19]. These values lead to the conclusion that boron could confer higher stability to the spinel.

(b) Boron with its capability to form coordinate bond with oxygen atoms could also make the metal–oxygen bond stronger, which is a prime requirement for providing better cyclability.

3.2.3. Diffusion coefficient of lithium

The open circuit voltage (OCV) corresponding to different lithium content in $Li_xB_yMn_{2-y}O_4$ ($y = 1/3$, $1/6$), along with SR-parent spinel, is represented in Fig. 11. The patterns show a smooth drop in OCV with lithium content in the spinel, implicit of its single-phase behavior, constituting a solid solution at all level of lithium insertion. Further higher level of boron substitution leads realization of higher OCV. The OCV reaches a higher value at 0.5 Li content in $LiB_{1/3}Mn_{5/3}O_4$ as it is near the end of Mn^{3+} depletion.

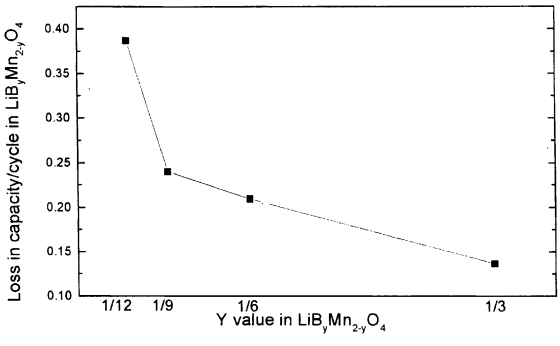

Fig. 10. Capacity loss in cells with SR-$LiB_yMn_{2-y}O_4$ ($y = 1/3$, $1/6$, $1/9$ and $1/12$).

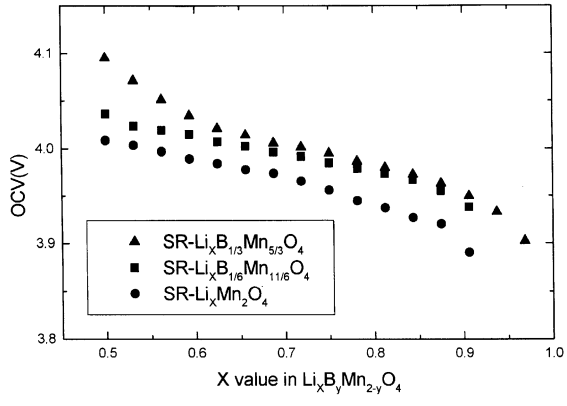

Fig. 11. Dependence of open circuit voltage of cells with SR-$Li_xB_yMn_{2-y}O_4$ ($y = 0$, $1/3$ and $1/6$) with different x values.

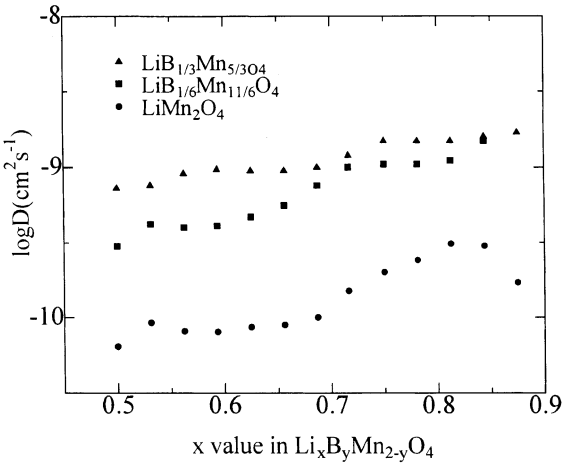

Fig. 12. Dependence of log of diffusion coefficient of Li in cells with SR-$Li_xB_yMn_{2-y}O_4$ ($y = 0$, $1/3$ and $1/6$) for different x values.

Fig. 12 shows the variation of logarithmic diffusion coefficient values of Li in $Li_xB_yMn_{2-y}O_4$ ($y = 1/3$ and $1/6$) along with SR-parent spinel for comparison. The curves show that the substituted spinel, in general, show diffusion coefficient values $\sim 10^{-9}$ cm^2 s^{-1}, which is around one order of magnitude greater than the parent spinel, $\sim 10^{-10}$ cm^2 s^{-1}. Since the atomic size of boron is smaller than the other cations in the spinel oxide, a doubt arises on its position as to whether it got substituted at 8*a* site of the tetrahedron or 16*d* site of the octahedron in the cubic spinel. If it got substituted at 8*a* site, the intermolecular diffusion path 8*a*–16*c*–8*a* will be obstructed by the presence of boron. An improvement in apparent diffusion coefficient value of lithium over the parent spinel has been observed in other metal-substituted lithium manganese oxide $LiM_yMn_{2-y}O_4$ (M = Cr, Co, Al) [14,22]. This could certainly support that boron got substituted at 16*d* site, as this position does not obstruct the diffusion pathway.

4. Conclusion

(a) The boron-substituted spinels synthesized through the solution route (precursor powder calcined at 500°C) provides higher capacity and better cyclability.

(b) SR-B spinel calcined at 600°C suggests that boron got eliminated at this temperature, leading to simultaneous formation of pure spinel phase and lithium borate glass formation. Formed spinel undergoes distortion to tetragonal configuration at 750°C. The smaller radius of boron (~ 0.2 Å) could not effectively influence the surrounding oxygen spheres to result in compact spinel structure, to provide stability at higher temperature.

(c) The smooth drop in OCV and the high diffusion coefficient of lithium suggest that boron got substituted at 16*d* site of the cubic spinel in the SR-B spinel, with calcinations temperature at 500°C.

(d) Finally, as the compound $LiB_{1/9}Mn_{17/9}O_4$ inherits good electrochemical behavior and constitutes less toxic elements, it can be considered as a promising positive electrode material for lithium ion battery.

Acknowledgements

One of the authors, A. Veluchamy, wishes to thank Dr. M. Watanabe for having arranged financial support through NIRIM, STA, Japan and for carrying out this work at the Tokyo Institute of Technology. Thanks are also due to Mr. S.S. Kim, a doctoral course student, for his technical support during this period.

References

[1] C. Delmas, I. Saadoune, A. Rougier, J. Power Sources 44 (1993) 595.
[2] T. Ohzuku, A. Ueda, M. Nagayama, Y. Iwakoshi, H. Komori, Electrochim. Acta 38 (1993) 1159.
[3] T. Nagaura, K. Tazawa, Prog. Batteries Sol. Cells 9 (1990) 20.
[4] K. Ozawa, Solid State Ionics 69 (1994) 212.
[5] M.M. Thackeray, A. de Kock, M.H. Rossouw, D. Liles, R. Bittihn, D. Hoge, J. Electrochem. Soc. 139 (1992) 363.
[6] M.Y. Saidi, J. Barker, R. Koksbang, Electrochim. Acta 41 (1996) 199.
[7] T. Ohzuku, M. Kitagawa, T. Hirai, J. Electrochem. Soc. 137 (1990) 769.
[8] J.M. Tarascon, D. Guyomard, Electrochim. Acta 38 (1991) 1221.
[9] J.M. Tarascon, W.R. McKinnon, F. Coowar, T.N. Boowmer, G. Amatucci, D. Guyomard, J. Electrochem. Soc. 141 (1994) 1421.

[10] D. Guyomard, J.M. Tarascon, Solid State Ionics 69 (1994) 222.
[11] M. Wakihara, G. Li, H. Ikuta, in: M. Wakihara, O. Yamamoto (Eds.), Lithium Ion Batteries. Kodansha-Wily VCH, Tokyo, 1998, p. 26.
[12] G. Li, H. Ikuta, T. Uchida, M. Wakihara, J. Electrochem. Soc. 143 (1996) 178.
[13] D. Song, H. Ikuta, M. Wakihara, Electrochemistry 68 (2000) 460.
[14] D. Song, H. Ikuta, T. Uchida, M. Wakihara, Solid State Ionics 117 (1999) 151.
[15] D. Song, G. Li, H. Ikuta, M. Wakihara, Electrochemistry 66 (1998) 1194.
[16] H.J. Kwon, S.S. Kim, G.B. Kim, D.G. Park, J. Mater. Sci. Lett. 15 (1996) 428.
[17] S.R.S. Prabaharana, S.S. Michaelb, C. Julien, Int. J. Inorg. Mater. 1 (1999) 21.
[18] S. Basu, W. Worrell, in: P. Vashishta, J.N. Mundy, G.K. Shenoy (Eds.), Fast Ion Transport, In Solids. Elsevier, North Holland, 1979, p. 149.
[19] I. Barin (Ed.), Thermo-Chemical Data on Pure Substance Substances. VCH Publishers, Weinheim, 1989, pp. 90–91.
[20] S. Wang, X. Huang, L. Chen, J. Mater. Chem. 10 (2000) 1465.
[21] A.R. West, Solid State Chemistry and Its Application. Wiley, New York, 1984, p. 270.
[22] M. Wakihara, L. Guohua, H. Ikuta, T. Uchida, Solid State Ionics 86–88 (1996) 907.